Author Manuscript

Author Manuscript

Author Manuscript

Author Manuscript

HHS Public Access

Author manuscript

Nat Cell Biol. Author manuscript; available in PMC 2015 November 01.

Published in final edited form as:

Nat Cell Biol. 2015 May ; 17(5): 678–688. doi:10.1038/ncb3157.

Matrix stiffness drives Epithelial-Mesenchymal Transition and tumour metastasis through a TWIST1-G3BP2 mechanotransduction pathway

Spencer C. Wei[1,2,7,#], **Laurent Fattet**[1,7], **Jeff H. Tsai**[1], **Yurong Guo**[3], **Vincent H. Pai**[1,2], **Hannah E. Majeski**[1,2], **Albert C. Chen**[5], **Robert L. Sah**[5], **Susan S. Taylor**[1,3,4], **Adam J. Engler**[5], and **Jing Yang**[1,6]

[1]Department of Pharmacology, University of California, San Diego, 9500 Gilman Drive, La Jolla, California, 92093-0819

[2]The Biomedical Sciences Graduate Program, University of California, San Diego, 9500 Gilman Drive, La Jolla, California, 92093-0819

[3]Howard Hughes Medical Institute, University of California, San Diego, 9500 Gilman Drive, La Jolla, California, 92093-0819

[4]Department of Chemistry and Biochemistry, University of California, San Diego, 9500 Gilman Drive, La Jolla, California, 92093-0819

[5]Department of Bioengineering, University of California, San Diego, 9500 Gilman Drive, La Jolla, California, 92093-0819

[6]Department of Pediatrics, University of California, San Diego, 9500 Gilman Drive, La Jolla, California, 92093-0819

Abstract

Matrix stiffness potently regulates cellular behavior in various biological contexts. In breast tumours, the presence of dense clusters of collagen fibrils indicates increased matrix stiffness and correlates with poor survival. It is unclear how mechanical inputs are transduced into transcriptional outputs to drive tumour progression. Here we report that TWIST1 is an essential mechano-mediator that promotes epithelial-mesenchymal transition (EMT) in response to increasing matrix stiffness. High matrix stiffness promotes nuclear translocation of TWIST1 by releasing TWIST1 from its cytoplasmic binding partner G3BP2. Loss of G3BP2 leads to constitutive TWIST1 nuclear localization and synergizes with increasing matrix stiffness to induce

Users may view, print, copy, and download text and data-mine the content in such documents, for the purposes of academic research, subject always to the full Conditions of use:http://www.nature.com/authors/editorial_policies/license.html#terms

*Correspondence should be addressed to J.Y. (jingyang@ucsd.edu).
[7]These authors contributed equally to this work.
[#]Current address: Department of Immunology, The University of Texas MD Anderson Cancer Center, 7455 Fannin Street, Houston, Texas, 77030

Author Contributions: S.C.W. and J.Y. conceived the project and wrote the manuscript. S.C.W. and L.F. performed most of the experiments and made the figures. J.H.T, Y.G., V.H.P, H.E.M., and A.C.C. contributed to the experimental work. R.L.S., S.S.T., and A.J.E. advised on experimental design. L.F., J.H.T., and A.J.E. revised the manuscript.

Competing Financial Interests: The authors declare no competing financial interests.

EMT and promote tumour invasion and metastasis. In human breast tumours, collagen fiber alignment, a marker of increasing matrix stiffness, and reduced expression of G3BP2 together predict poor survival. Our findings reveal a TWIST1-G3BP2 mechanotransduction pathway that responds to biomechanical signals from the tumour microenvironment to drive EMT, invasion, and metastasis.

Breast tumours are often detected by manual palpation, as they are more rigid than their surrounding normal tissue. This increase in tissue rigidity, or matrix stiffness, plays a significant role during tumour progression[1-5]. Organized collagen fiber alignment, which is a surrogate marker for increasing matrix stiffness in the tumour microenvironment, is associated with breast tumour progression[6-8]. The importance of mechanical forces in regulating cellular behaviors is also evident during embryogenesis[9-11]. For example, mesenchymal stem cells (MSCs) undergo lineage selection into either neurons or muscle and bone in response to distinct matrix elasticities[12]. The transcription co-activator YAP accumulates in the nucleus in stiffer matrices to allow osteogenic differentiation of MSCs[13]. How changes in the mechanical properties of extracellular matrix are converted into biochemical and transcriptional responses to direct tumour cell behavior remains unknown.

Studies have shown that human mammary epithelial cells form normal ductal acini on compliant matrices that recapitulate the stiffness of normal mammary glands. On matrices with increased rigidity similar to breast tumours, however, cells lose apical-basal polarity, form weaker junctions and invade through basement membrane[1,2]. These cellular changes in response to increasing stiffness resemble many morphological features associated with EMT, a developmental program also critical for tumour cell dissemination and metastasis[14,15]. During EMT, cells lose their epithelial characteristics, including cell junctions and polarity, and acquire a mesenchymal morphology and the ability to invade. The EMT program is orchestrated through a network of transcription factors, including TWIST1, TWIST2[16,17], SNAI1, SNAI2[18-20], ZEB1, and ZEB2[21,22]. Therefore, we set out to understand how matrix stiffness regulates the EMT molecular pathway to promote tumour invasion and metastasis.

Results

TWIST1 is essential for matrix stiffness-induced EMT and invasion

The basic Helix-Loop-Helix (bHLH) transcription factor, TWIST1, is essential for the ability of tumour cells to metastasize through activation of EMT and extracellular matrix degradation[23,24]. Mechanical forces induce Twist expression during Drosophila larval development[25], therefore, we asked whether increasing matrix stiffness regulates mammalian TWIST1 to promote EMT and tumour invasion. We employed a collagen-coated polyacrylamide (PA) hydrogel system with calibrated elastic moduli ranging from the ∼150 Pascals (Pa) of normal mammary glands to the ∼5700 Pa of breast tumour tissues[1,26] in a 3D Matrigel overlay culture system[27-29]. Non-transformed human MCF10A and tumourigenic mouse Eph4Ras mammary epithelial cells were used because unlike normal mammary epithelial cells *in vivo*[30], both cell lines endogenously express TWIST1, suggesting that genetic or epigenetic alterations predispose them to tumour

Author Manuscript Author Manuscript Author Manuscript Author Manuscript

Author Manuscript Author Manuscript Author Manuscript Author Manuscript

progression[24,31,32]. Both cells developed polarized ductal acini surrounded by intact basement membrane on compliant 150 Pa matrices. In contrast, at a high matrix stiffness of 5,700 Pa, cells presented a partial EMT phenotype (Fig. 1A), similar to the matrix stiffness-induced malignant phenotype described previously[1]. Notably, the intact basement membrane observed at low stiffness was destabilized at high matrix stiffness, consistent with previous observations that increasing matrix stiffness induces cellular invasion (Supplementary Fig. 1A)[1,2,33]. As loss of basement membrane integrity is a critical event during the metastatic cascade, we utilized this dramatic response as a functional readout of cellular invasion in conjunction with changes in EMT markers.

Using this system, we tested whether TWIST1 is required for induction of EMT and invasion in response to high matrix stiffness. We generated Eph4Ras and MCF10A cells expressing shRNAs against *TWIST1* and tested their mechanosensing competence (Fig. 1B and Supplementary Fig. 1B-D). Knockdown of *TWIST1* prevented the invasive phenotype at 5700 Pa; instead, these cells formed basally polarized acini with strong junctional E-cadherin on rigid matrices (Fig. 1C-F and Supplementary Fig. 1E). Importantly, knockdown of *Twist1* prevented stiffness-induced basement membrane destabilization, as shown by basal Laminin V staining (Fig. 1E), demonstrating that matrix stiffness-induced invasion is *Twist1*-dependent. Since high stiffness alone was not sufficient to induce a complete EMT (Fig. 1F), we investigated whether TWIST1 is also required for the induction of a full EMT by mechanical signals in concert with the EMT-inducing biochemical signal TGF-β[34]. Consistent with published data[35], although TGF-β was not sufficient to induce EMT on soft matrix, rigid matrix together with TGF-β triggered a complete EMT, evidenced by both immunostaining and qPCR analysis of EMT markers (Fig. 1G and Supplementary Fig. 1F and 1G). Importantly, knockdown of *Twist1* completely blocked induction of EMT by TGF-β at high matrix stiffness and rescued acinar development (Fig. 1G). Together, these data indicate an essential role for TWIST1 in mediating matrix stiffness-induced EMT and invasion.

As the EMT program is orchestrated synergistically by a number of EMT-inducing transcription factors, we next aimed to understand how the EMT transcription program is regulated by matrix stiffness and TGF-β. The mRNA levels of EMT-inducing transcription factors, *Twist1*, *Snai1, Snai2, Zeb1,* and *Zeb2* did not change significantly in response to changes in matrix stiffness alone (Fig. 1H-1L). Upon TGF-β treatment, only *Snai1* mRNA is drastically induced in a Twist1-independent manner (Fig. 1I), as reported previously[32]. However, without Twist1, TGF-β-induced *Snai1* expression alone could not induce even a partial EMT or any invasive phenotype on soft or hard matrices (Fig. 1G). The mRNA expression levels of *Snai2, Zeb1,* and *Zeb2* were significantly dampened upon *Twist1* knockdown (Fig. 1J-1L), further supporting a key role of TWIST1 in regulating EMT gene response. These data suggest that TWIST1-dependent mechanotransduction, together with induction of *Snai1* by TGF-β, is required to induce a complete EMT at high matrix stiffness.

Matrix stiffness regulates TWIST1 nuclear localization

We next aimed to understand how TWIST1 is regulated by matrix stiffness to mediate EMT and invasion. Since Drosophila *Twist* mRNA expression is induced by mechanical forces[25],

Author Manuscript Author Manuscript Author Manuscript Author Manuscript

we examined TWIST1 mRNA and protein expression under various matrix rigidities and found no differences (Fig. 2A and 2B). Surprisingly, immunostaining showed that TWIST1 was largely cytoplasmic on the compliant matrix of 150Pa and translocated into the nucleus on the rigid matrix of 5700Pa. High stiffness-induced nuclear translocation of TWIST1 was observed in human MCF10A and mouse Eph4Ras cells (Fig. 2C), and in MCF10DCIS and Bt-549 human breast cancer cells (Fig. 2D and 2E), suggesting that nuclear translocation of TWIST1 is a conserved response to increasing matrix stiffness. These results suggest that matrix stiffness could directly impinge upon the EMT program by controlling TWIST1 nuclear translocation.

TWIST1 subcellular localization is regulated by a distinct mechanotransduction pathway independent of YAP

We next tested whether integrin activation is necessary for TWIST1 nuclear localization at high matrix stiffness since mechanosensing responses to matrix stiffness are mediated in part through clustering and activation of integrins[1,36]. Treatment with a β1-integrin blocking antibody (AIIB2) prevented nuclear translocation of TWIST1 and blocked the invasive phenotype induced by high matrix stiffness (Fig. 3A)[1,2], further supporting a critical role of TWIST1 in mediating matrix stiffness-induced EMT and invasion. Notably, blockade of β1-integrin activation also prevented nuclear localization of YAP, which was recently identified as one of the few known mechano-responsive transcription regulators[13]. Therefore, integrin activation is critical to the mechanoregulation of both Twist1 and YAP.

Next we asked whether TWIST1 and YAP are regulated by similar mechano-regulatory machineries. Since matrix stiffness also affects cell shape, we sought to distinguish their impacts on TWIST1 nuclear localization. First, we used micropatterning to selectively alter cell shapes without changing underlying matrix rigidity. Restrictive patterns with areas of 225 μm^2 and 400 μm^2 prevented any cell spreading, in contrast, MCF10A cells on unpatterned regions were able to spread effectively (Fig. 3B). TWIST1 nuclear localization was not affected by changes in cell shape in either MCF10A or Eph4Ras cells (Fig. 3B-D and Supplementary Fig. 2). To confirm that micropatterning-restriction of cell spreading was effective, we also examined the localization of YAP. In contrast to TWIST1, YAP subcellular localization was responsive to changes in cell shape (Fig. 3C and 3D), consistent with previous reports that YAP localization is sensitive to any changes in actin cytoskeleton[13,37]. This difference suggests the existence of distinct mechanoregulatory mechanisms for TWIST1 and YAP. These data also suggest that matrix stiffness directly regulates TWIST1 subcellular localization independently of changes in cell shape.

Because TWIST1 protein subcellular localization could be regulated by nuclear transport, we explored whether TWIST1 nuclear import and export might be regulated by matrix stiffness. Treatment of MCF10A cells with Leptomycin B, a nuclear export inhibitor[38], did not promote nuclear accumulation of TWIST1 on compliant matrices (Fig. 3E, upper panel). In contrast, YAP accumulated into the nucleus upon inhibition of nuclear export (Fig. 3E, lower panel). Therefore, similar to the micropatterning experiment, inhibition of nuclear export differentially affected matrix stiffness regulation of TWIST1 and YAP, supporting the existence of distinct Twist1 and YAP mechanotransduction pathways. Furthermore, as

Author Manuscript Author Manuscript Author Manuscript Author Manuscript

TWIST1 contains two functional nuclear localization sequences[39], these results suggest that TWIST1 is likely to be actively anchored in the cytoplasm on compliant matrices, therefore preventing nuclear translocation.

Matrix stiffness regulates the interaction between TWIST1 and G3BP2 to control TWIST1 subcellular localization

To understand the molecular mechanism underlying TWIST1 cytoplasmic retention, we used mass spectrometry analysis to identify TWIST1-binding proteins that anchor TWIST1 in the cytoplasm (Supplementary Fig. 3A). Ras GTPase-activating protein-binding protein 2 (G3BP2) stood out as a promising candidate based on previous studies showing that G3BP2 regulates cytoplasmic retention of MDM2 and NFKBIA[40,41]. We confirmed that both endogenously and exogenously expressed TWIST1 co-immunoprecipitated with endogenous G3BP2 (Fig. 4A and Supplementary Fig. 3C). Previous studies identified a region of NFKBIA responsible for binding to G3BP2[41]. Sequence alignment of this G3BP2-interacting region of NFKBIA with TWIST1 and MDM2 revealed a consensus G3BP2-binding motif, Q-X-X-X-E-L-Q-[ET]-X-[KR]-[LPV] (Fig. 4B). Interestingly, this G3BP2-binding motif is highly conserved among vertebrate Twist1 proteins, but to a significantly lesser degree in *Drosophila* in which Twist expression, rather than localization, is regulated by mechanical cues[25] (Fig. 4C). Deletion of this motif (QT mutant) in Twist1 abolished its interaction with G3BP2 (Fig. 4D). Consistent with its putative role as a cytoplasmic anchoring protein, G3BP2 was observed only in the cytoplasm in Eph4Ras, MCF10A, and Bt-549 cells at all matrix rigidities (Fig. 4E and Supplementary Fig. 3B). Together, these data show that G3BP2 binds to TWIST1 through the conserved G3BP2-binding motif on vertebrate TWIST1 proteins.

To directly test whether matrix stiffness regulates Twist1-G3BP2 interaction, we utilized *in situ* proximity ligation assay (PLA) to examine the interaction of endogenous Twist1 and G3bp2 proteins in 3D acinar cultures of Eph4Ras cells. PLA technology directly detects endogenous Twist1/G3bp2 interactions with high specificity and sensitivity in intact acini using antibodies against Twist1 and G3bp2. Indeed, at 150Pa a strong PLA signal, indicating Twist1/G3bp2 interaction, was specifically enriched in the cytoplasm. In contrast, very little PLA signal was detected at 5700Pa, indicating that Twist1 is released from G3bp2 and translocates into the nucleus at high matrix rigidity (Fig. 4F and 4G). To understand whether Twist1-G3bp2 interaction is specifically regulated by matrix stiffness, and not by secondary changes in cell polarity or adherens junctions due to matrix stiffness-induced EMT, we examined Twist1-G3bp2 interaction in single cells devoid of apical-basal polarity and mature adherens junctions. PLA analysis in single cells detected strong interaction between G3bp2 and Twist1 in the cytoplasm at low stiffness, but not at high stiffness (Fig. 4H and 4I), identical to what we observed in mammary organoids with mature adherens junctions and polarity. These experiments demonstrate that matrix stiffness directly regulates the interaction between Twist1 and G3bp2 to control Twist1 subcellular localization.

Next, we investigated how the interaction between TWIST1 and G3BP2 could be regulated in response to changes in matrix stiffness. Interestingly, the tyrosine residue Y103 (Y107 in

Author Manuscript
Author Manuscript
Author Manuscript
Author Manuscript

murine Twist1), which lies within the identified G3BP2 binding motif of human TWIST1, is predicted as a potential phosphorylation site. This provided a very attractive potential mechanism by which increased matrix stiffness activates integrins and then signals through tyrosine kinases to release TWIST1 from G3BP2. Supportive of this possibility, mass spectrometry analysis of a human lung adenocarcinoma cell line reveals phosphorylation of Y103 on endogenous TWIST1[42], albeit with no known functional consequence. Interestingly, the phospho-deficient Y107F Twist1 mutant co-immunoprecipitated with G3BP2 with similar efficiency as wild-type Twist1 but the interaction between the phospho-mimetic Y107E Twist1 mutant and G3BP2 was markedly attenuated (Fig. 4J). These data strongly suggest that increasing matrix stiffness could disrupt Twist1-G3BP2 binding through phosphorylation of Y107 within the G3BP2-binding motif of Twist1.

Loss of G3BP2 cooperates with increasing matrix stiffness to promote TWIST1 nuclear localization and EMT

We next asked whether G3BP2 is functionally required for TWIST1 cytoplasmic retention in compliant matrices. We used shRNAs to knock down *G3BP2* expression and determined the impact on TWIST1 localization (Fig. 5A, 5E and Supplementary Fig. 4A). For both MCF10A and Eph4Ras cells on compliant matrices, knockdown of *G3BP2* resulted in nuclear accumulation of TWIST1, suggesting that G3BP2 is necessary for cytoplasmic sequestration of TWIST1 in response to low matrix stiffness (Fig. 5B and Supplementary Fig. 4B). TWIST1 nuclear localization at high matrix stiffness was not affected by knockdown of *G3BP2*, consistent with our model in which G3BP2 and TWIST1 dissociate at high matrix stiffness. In further support of distinct mechanoregulation of TWIST1 and YAP, knockdown of *G3BP2* did not affect YAP localization (Supplementary Fig. 4D). These data strongly support a critical role of G3BP2 in regulating TWIST1 subcellular localization in response to matrix stiffness.

To determine the impact of G3BP2 loss on EMT and invasion, we cultured Eph4Ras cells on a gradient of polyacrylamide hydrogels with elasticities ranging from 150Pa to 5700Pa in 3D culture. *G3bp2* knockdown and the resulting constitutive Twist1 nuclear localization significantly increased the percentage of invasive acini at matrix rigidities ranging from 150Pa to 670Pa. Importantly, loss of *G3bp2* and increasing matrix stiffness synergistically resulted in destabilization of basement membrane, an EMT phenotype, and invasion of cells into the surrounding ECM (Fig. 5C and 5D). The EMT phenotype was characterized by down-regulation of E-cadherin and disruption of basement membrane as shown by Laminin V staining (Fig. 5C). Furthermore, *G3bp2* knockdown repressed expression of E-cadherin and induced expression of Vimentin (Fig. 5G and 5H). To determine whether the EMT phenotype resulting from *G3bp2* knockdown is dependent on Twist1, we knocked down both *Twist1* and *G3bp2* and found that the EMT and invasive phenotype were significantly suppressed compared to cells that were only depleted of G3bp2 (Fig. 5I). *Snai2*, a direct transcription target of TWIST1[43], was induced following *G3bp2* knockdown ; in contrast, double knockdown of *G3bp2* and *Twist1* blocked *Snai2* induction, suggesting that the effects of *G3bp2* knockdown are dependent on *Twist1*(Fig. 5F and Supplementary Fig. 4C). These data indicate that G3BP2 directly impacts EMT and invasion in response to matrix stiffness and provide a mechanism by which the TWIST1-G3BP2 mechanotransduction pathway can

Author Manuscript Author Manuscript Author Manuscript Author Manuscript

facilitate tumour invasion. Furthermore, it suggests that down-regulation of G3BP2 expression in tumour cells could cooperate with increasing matrix stiffness in the tumour microenvironment to facilitate tumour invasion and metastasis.

Loss of G3BP2 promotes tumour invasion and metastasis *in vivo*

To test the role of G3BP2 in tumour progression *in vivo*, we employed a human xenograft tumour model of comedo ductal carcinoma *in situ*, the MCF10DCIS cell line[44], which is a derivative of MCF10A cells expressing oncogenic Ras. This xenograft model recapitulates the development of ductal carcinoma in situ (DCIS) in human breast cancer. Concordant with our results in Eph4Ras and MCF10A mammary epithelial cells, knockdown of *G3BP2* in conjunction with increasing matrix stiffness promoted TWIST1 nuclear localization and an invasive phenotype in MCF10DCIS cells in 3D culture, indicating that the TWIST1-G3BP2 mechanotransduction pathway is intact in this model (Fig. 6A, 6B, and Supplementary Fig. 5). We injected these cells into the mammary fat pads of NOD/SCID mice and allowed tumour formation for 7 weeks. There was no significant difference in the weight of control and G3BP2 shRNA primary mammary tumours (Fig. 6C). Immunostaining confirmed significantly lower levels of G3BP2 in tumours with *G3BP2* knockdown (Fig. 6D). Interestingly, in control tumours, αSMA-positive mesenchymal cells were largely present at the edge of the tumour; in contrast, these cells often infiltrated into the intratumoural region in G3BP2 shRNA tumours, a phenotype associated with the progression of DCIS to invasive ductal carcinoma (Fig. 6D).

We next examined whether knockdown of G3BP2 affects tumour invasion and metastasis. Tumours expressing *G3BP2* shRNAs presented not only local invasion into the surrounding mammary tissue, but also regional invasion into the nearby peritoneal wall, visualized as GFP positive tumour cells in these regions (Fig. 6E and 6F). More importantly, tumours expressing *G3BP2* shRNAs consistently presented with a striking increase in the number of distant metastases in the lungs compared to tumours expressing a control shRNA (mean increase: 15 and 65-fold for G3BP2 shRNA6 and shRNA8 versus control, respectively) (Fig. 6G, 6H). Together, these results strongly support a key role for G3BP2 in suppressing tumour invasion and metastasis *in vivo*.

Downregulation of G3BP2 and increasing collagen organization synergistically predict poor outcome in breast cancer patients

We next investigated whether the TWIST1-G3BP2 mechanotransduction pathway has a significant role in human cancer progression. We first analyzed The Cancer Genome Atlas (TCGA) breast cancer (TCGA_BRCA_G4502A_07_3) dataset and observed a decrease in overall survival in patients with tumours with low G3BP2 expression (Supplementary Fig. 6A and 6B). Furthermore, consistent with a role in preventing EMT and invasion, we observed that G3BP2 protein expression was restricted to the luminal epithelial cells in normal human breast and colon tissues (Fig. 7A, and Supplementary Fig. 6D). We next analyzed G3BP2 expression and collagen organization in a cohort of 152 Stage-3 breast tumours from the NCI Cancer Diagnosis Program (Fig. 7B). We analyzed collagen fiber alignment by Second Harmonic Generation imaging (SHG) and used it as a surrogate marker for tissue rigidity. In agreement with previous publications[6-8,45,46], Stage-3 patients

Author Manuscript
Author Manuscript
Author Manuscript
Author Manuscript

presenting stiffer tumours (organized collagen structures) had a median recurrence-free survival time of 31 months compared to 49 months in patients with more compliant tumours (disorganized collagen) (p=0.0014) (Supplementary Fig. 6C). Importantly, the level of G3BP2 expression, together with matrix stiffness, could further stratify these patients to predict outcome (Fig. 7C). Patients with disorganized collagen/G3BP2^{high} tumours had dramatically improved outcomes with 10-year recurrence-free survival rate of 46.4% compared to 10.1% of patients with organized collagen/G3BP2^{low} tumours. Patients whose tumours presented either low G3BP2 or organized collagen fibers had intermediate survival outcomes (31.18% and 33.33% 10-year recurrence free survival, p=0.0284), reflective of the cooperative effect of G3BP2 loss and increasing matrix stiffness on tumour progression. The association between downregulation of G3BP2 and poor prognosis was independent of tumour grade or ER status (Supplementary Fig. 6E and 6F). Concordant with data from 3D culture and animal tumour models, these results demonstrate that increasing rigidity in the tumour microenvironment, in concert with down-regulation of G3BP2, promotes human breast tumour progression.

Discussion

In summary, we demonstrate that increasing matrix stiffness in the tumour microenvironment directly activates EMT, tumour invasion, and metastasis through the EMT-inducing transcription factor TWIST1. This mechanotransduction pathway may have important implications in breast tumours, as G3BP2 loss and tissue rigidity act synergistically to promote tumour progression. Given that matrix stiffening and ECM reorganization has been observed in many human tumour types[47], the Twist1-G3BP2 mechanotransduction pathway warrants further investigation as a key mode of EMT activation as well as for therapeutic applications.

Mechanistically, our study reveals a molecular pathway directly linking mechanical forces with transcriptional regulation of the EMT program. Our findings suggest a model in which increasing matrix stiffness induces integrin-dependent phosphorylation events and release of TWIST1 from its cytoplasmic anchor G3BP2 to enter the nucleus and drive transcriptional events of EMT and invasion. Notably, to our knowledge, low stiffness and integrin disengagement are the only conditions in which cytoplasmic retention of TWIST1 are observed, thus providing a unique mode of EMT regulation[48]. Interestingly, our analyses showed that matrix stiffness regulates TWIST1 and YAP/TAZ through distinct molecular mechanisms, suggesting that multiple mechanotransduction pathways exist. We found that the TWIST1-G3BP2 signaling axis is only responsive to matrix stiffness and is independent of cell shape, cell polarity, and adherens junction; in contrast, YAP/TAZ are sensitive to all these factors. Currently, the complete molecular pathways that transmit the mechanical signals from extracellular matrix to either the YAP/TAZ or TWIST1 signaling axis remain to be elucidated. Understanding the similarities and differences between the YAP/TAZ versus TWIST1 mechanotransduction pathways will provide further insight on how different mechanical cues are interpreted into unique biological responses. Given the importance of mechanoregulation in embryonic morphogenesis, such information would have broad implications not only in tumour progression, but also in development.

Author Manuscript Author Manuscript Author Manuscript Author Manuscript

Online Methods

Cell culture

MCF10A cells were grown in DMEM/F12 media supplemented with 5% horse serum, 20 ng/ml human EGF, 10 μg/ml insulin, 0.5 μg/ml hydrocortisone, penicillin, streptomycin, and 100 ng/ml cholera toxin (Sigma-Aldrich). Eph4Ras cells were cultured as previously described in MEGM (Lonza) mixed 1:1 with DMEM/F12 media supplemented with 10 ng/ml human EGF, 10 μg/ml insulin, 0.5 μg/ml hydrocortisone, penicillin, and streptomycin[24]. Bt-549 cells were grown in RPMI 1640 supplemented with L-glutamine, penicillin, streptomycin, 10% fetal bovine serum, and 1μg/ml insulin. All cell lines were tested for mycoplasma contamination.

Generation of stable knockdown cell lines

Stable gene knockdown cell lines were generated using lentiviral plasmid vectors. Briefly, shRNA target constructs were introduced by infection with lentiviruses. Concentrated viral supernatants were applied to target cells with 6 μg/ml protamine sulfate. Infected cells were then selected for with 2 μg/ml puromycin or blasticidin.

Polyacrylamide hydrogel preparation

Hydrogels were prepared as previously described on No. 1 12 mm and 25 mm coverslips were utilized[49]. Briefly, No. 1 glass coverslips were etched using 0.1 N NaOH, functionalized using 3-aminopropyltriethoxysilane (Sigma-Aldrich), rinsed with dH20, incubated in 0.5% gluteraldehyde in PBS, dried, and then acrylamide/bis-acrylamide mixtures polymerized between the functionalized coverslip and a glass slide coated with dichlorodimethylsiloxane (Sigma-Aldrich). Polyacrylamide coated coverslips were then washed twice with dH20, incubated with 1 mM Sulfo-SANPAH (Thermo Scientific Pierce) in HEPES buffer under 365 nm UV light for 10 minutes, rinsed twice with 50 mM HEPES pH 8.5 buffer, incubated at 37°C overnight with rat tail Collagen I (Millipore) in 50 mM HEPES pH 8.5 buffer, rinsed twice in 50 mM HEPES pH 8.5 buffer, and sterilized.

3-dimensional (3D) cell culture

MCF10A and Eph4Ras cells grown in 3D cell culture as previously described[29]. Briefly, Eph4ras cells were seeded on hydrogels in 2% Matrigel (BD Biosciences) MEGM mixed 1:1 with DMEM/F12 and MCF10A cells seeded similarly in 2% Matrigel DMEM/F12 media supplemented with 2% horse serum, 5 ng/ml human EGF, 10 μg/ml insulin, 0.5 μg/ml hydrocortisone, penicillin, streptomycin, and 100 ng/ml cholera toxin.

3D confocal microscopy

Protocol adapted from method described by Debnath *et al*[29]. In brief, cells were fixed with 2% paraformaldehyde (PFA) for 20 minutes at room temperature, permeabilized with PBS-0.5% Triton X-100, quenched with 100 mM PBS-glycine, and then blocked with 20% goat serum-immunofluorescence (IF) buffer (130 mM NaCl, 7.7 mM NaN_3, 0.1% BSA, 0.2% Triton-X100, 0.05% Tween-20, PBS). Samples were incubated with primary antibodies overnight in 20% goat serum-IF buffer, washed 3 times with IF buffer, incubated

Author Manuscript Author Manuscript Author Manuscript Author Manuscript

with secondary antibodies for 1 hour, washed 3 times with IF buffer, counterstained for nuclear for 15 minutes (5 ng/ml DAPI or TO-PRO-3), washed once with PBS, and mounted with Slow Fade Gold (Invitrogen). Confocal images were acquired using an Olympus FV1000 with 405, 488, 555, and 647 laser lines. Images were linearly analyzed and pseudo-colored using ImageJ analysis software.

Invasive Acini Quantification

Invasive acini were quantified using brightfield images with at minimum 5 random low-magnification fields being analyzed per condition per experiment. Acini were scored as either normally developed acini or acini that adopted a spread and invasive phenotype.

Second Harmonic Generation Microscopy

5 micron formalin-fixed paraffin embedded sections were re-hydrated and imaged using a multi-photon Leica SP5 confocal microscope using a TI-Sapphire light source and a 20× water-immersion objective at 880 nm. Fields were acquired using resonant scanning mode, line averaging, and frame accrual. IF staining was sequentially imaged using scanning laser confocal microscopy. The scoring rubric (which was defined prior to blinded scoring) for SHG analysis was defined as “organized collagen” in tumours having prominent linearized collagen fibers (with a circularity close to 0) or as “disorganized collagen” in tumours having either collagen fibers with high degree of circularity (i.e. curved) or low/no SHG signal.

Tumour tissue microarrays

National Cancer Institute Cancer Diagnosis Program Stage 3 breast cancer progression tumour tissue microarrays (TMA) were stained for G3BP2 by immunofluorescence for retrospective analysis. TMAs were concurrently imaged by confocal microscropy and SHG. Cores that were missing, damaged, or without detectable tumour cells were omitted from analyses. G3BP2 was scored blindly according to the following rubrics. G3BP2 expression was scored 0 for no detectable expression, 1 for very weak expression, 2 for moderate expression in greater than 75% of tumour cells, and 3+ for strong expression in greater than 75% of tumour cells. Data for ER status and tumour grade were included in the annotated dataset provided by the NCI CDP.

Antibodies

Primary antibodies include anti-β-actin (Abcam, ab13822, 1:3000), anti-E-cadherin (BD, 610182, 1:200 for immunostaining, 1:1000 for Western blotting), anti-E-cadherin (Abcam, ab11512, Decma-1, 1:200), anti-G3BP2 (Sigma-Aldrich , HPA018425, 1:200, 1:1000), anti-Fibronectin (Sigma-Aldrich, F3648, 1:200), anti-Integrin α6 (Millipore, MAB1378, NKI-GoH3, 1:200), anti-human Laminin V (Chemicon, D4B5, 1:200), anti-mouse Laminin V (kind gift from M. Aumailley, 1:1000), anti-Twist1 (Santa Cruz, ab50887, Twist2C1a, 1:100, 1:1000), Rabbit anti-Twist1 (Sigma-Aldrich, T6451, 1:1000), 5b7 mouse anti-Twist1 hybridoma cell line (1:1000), anti-YAP1 (Santa Cruz, H-125, 1:100). AIIB2 hybridoma supernatant was used for β1 integrin blocking experiments (Developmental Studies Hybridoma Bank, 1:1000). Secondary fluorescent antibodies used include anti-mouse, anti-

Author Manuscript Author Manuscript Author Manuscript Author Manuscript

rat, and anti-rabbit conjugated with Alexafluor 488, 546, and 647 (Life Technologies). Secondary horseradish peroxidase (HRP) conjugated antibodies used include anti-mouse, anti-rabbit, and anti-chicken (Jackson Immunoresearch).

Immunoprecipitation

Cells were lysed using a 2-step protocol adapted from Klenova et al [50]. Cells were directly lysed with lysis buffer (20 mM Tris-HCl, 1% Triton X-100, 10 mM $MgCl_2$, 10 mM KCl, 2 mM EDTA, 1 mM NaF, 1 mM sodium orthovandate, 2.5 mM β-glycerolphosphate, 10% glycerol, ph 7.5), scraped off the culture dish, sonicated, supplemented to 400 mM NaCl, sonicated, and diluted to 200 mM NaCl. Antibodies were conjugated to protein G beads (Invitrogen), crosslinked using disuccinimidyl suberate (Thermo Scientific Pierce) as per manufacturer's protocol, incubated with lysates overnight at 4 degrees Celsius, washed eight times with IP lysis buffer supplemented with 200 mM NaCl, and eluted using 50 mM DTT LDS sample buffer at 95 degrees Celsius for 15 minutes. 5B7 mouse hybridoma concentrated supernatant was used. For immunoprecipitation of exogenously transfected Myc-Twist1, 293T cell lysates were harvested 48 hours after transfection and subjected to 2-step lysis protocol. Immunoprecipitation was performed using anti-Myc antibody (9E10) crosslinked to protein A agarose beads (Invitrogen).

Mass Spectrometry

The gel bands were excised and cut into 1×1-mm pieces. In gel digestion and extraction were done as previously described[51]. The peptides were separated on reversed-phase HPLC analytical column (360 μm O.D. × 50 μm I.D., ODS-AQ 5 μm, 10 cm) with an integrated tip (1-2 μm) with a gradient of 0-40%B for 30 minutes, 40-100%B for 5 minutes, 100%-0%B for 2 minutes, and 0%B for 15 minutes using Agilent 1100 quarternary pump and eluted into LTQ Orbitrap. LTQ Orbitrap was operated in a data-dependent mode. MS was acquired in Orbitrap with a resolution of 15000 and MS/MS was acquired in LTQ. Tandem mass spectra were searched against the IPI mouse database using Bioworks with the following modification: differential Methionine 15.9949. For peptides xcorr cut off filter of 1.5 for +1, 2.0 for +2 and 2.5 for +3 was applied, and identified peptides were confirmed by manually inspecting the MS/MS spectra.

Micropatterning

Micropatterned coverslips were designed with and produced by CYTOO (http://www.cytoo.com/). Square micropatterns were produced in blocks with a 90μm pitch between each pattern with a block period of 1300 μm. Each pattern block was produced in duplicate on each coverslip. Activated coverslips were coated with 20 μg/ml rat tail collagen I for 2 hours at room temperature. Cells were then seeded for 6 hours and then fixed for analysis by confocal microscopy. At least 25 random single cells from 5 random fields were analyzed per condition.

Motif Sequence Alignment

Sequences were aligned using ExPASy SIB bioinformatics portal[52].

Author Manuscript
Author Manuscript
Author Manuscript
Author Manuscript

Proximity Ligation Assay

Cells were 3D cultured on PA gels for 20 hours or 6 days and fixed and processed as described for immunofluorescence before performing Duolink PLA (Sigma-Aldrich) as per manufacturer's protocol. Briefly, mouse anti-Twist1 (Abcam, ab50887, Twist2C1a, 1:150) and rabbit anti-G3BP2 (Sigma-Aldrich, HPA018425, 1:600) primary antibodies were used to detect endogenous proteins and subsequently recognized using species specific plus and minus PLA oligonucleotide conjugated probes at 37°C for 60 minutes. Interacting probes were then ligated at 37°C for 30 minutes and detected by polymerase mediated amplification at 37°C for 100 minutes and subsequently analyzed by fluorescent confocal microscopy. For analysis of formed day 6 acini a minimum 50 cells from 5 random fields were quantified per condition. For analysis of single cells seeded for 20 hours a minimum of 25 cells from 5 random fields were quantified per condition. To quantify PLA signal images were thresholded using ImageJ analysis software. The area with positive PLA signal was then quantified and divided by the number of cells examined.

Xenograft Tumour Assay

All animal care and experiments were approved by the Institutional Animal Care and Use Committee of the University of California, San Diego. 1.0×10^6 MCF10DCIS cells suspended in 15 μl Matrigel (BD Biosciences) were injected bilaterally into the inguinal mammary fat pads of 8 week-old female SCID-beige mice. No statistical method was used to predetermine sample size and the experiments were not randomized. Mice were sacrificed and tumour burden analyzed at 7 weeks post tumour implantation. Mice were dissected and tumour invasion assessed *in situ* using a fluorescent dissection scope (Leica Microsystems). The investigators were not blinded to allocation during experiments and outcome assessment.

TCGA Dataset Analysis

The TCGA breast cancer gene expression dataset (TCGA BRCA G4502A_07_3) was downloaded from the UCSC Cancer Genome Browser (https://genome-cancer.ucsc.edu/). Samples were stratified by G3BP2 expression, with G3BP2^{high} and G3BP2^{low} samples with expression above and below mean G3BP2 expression, respectively. Overall patient survival in each group was then analyzed.

Statistical Analysis

All p-values derived from Student's T-test using unpaired two-tailed analysis with Welch's correction, unless otherwise noted. Error bars denote standard deviation unless otherwise noted. Kaplan-Meier survival curves were analyzed by Cox-Mantel Log-rank analysis. Contingency tables were analyzed using Fisher's Exact analysis. Statistical significance was defined as $P < 0.05$, with regard to the null hypothesis. All qualitative data shown using representative data were repeated in at least 3 independent experiments.

Real-time PCR

RNA was extracted from cells using RNeasy Mini and Micro Kit (Qiagen). cDNA was generated using random hexamer primers and cDNA Reverse Transcription Kit (Applied

Author Manuscript
Author Manuscript
Author Manuscript
Author Manuscript

Biosystems). Expression values were generated using ddCt values normalized to GAPDH. Experiments were performed in biological and technical triplicate using 7500 Fast (Applied Biosystems) and CFX Connect (Bio-Rad) real-time PCR detection systems. For data analysis in each comparison (one shRNA vs. the control shRNA), unpaired two-tailed Student's T-tests with Welch's correction was used to determine statistical significance.

Murine primer sequences:

Twist1 (CAGCGGGTCATGGCTAAC, CAGCTTGCCATCTTGGAGTC),

G3bp2 (CCCGAGTATTTGCACAGGTT, TCACTCAAGGTTGCATGAGC),

Snai1 (AAGATGCACATCCGAAGCC, CGCAGGTTGGAGCGGTCAGC),

Snai2 (ATGCCCAGTCTAGGAAATCG, CAGTGAGGGCAAGAGAAAGG),

Zeb1 (TGATGAAAACGGAACACCAGATG, GTTGTCCTCGTTCTTCTCATGG),

Zeb2 (TGAAGAGAACTTTTCCTGCCCT, ATTTGGTGCTGATCTGTCCCT),

Cdh1 (GGGTGAATTCCCAAAGAACC, TGGCAATGGCTTCTCTATCC),

Vim (CGGCTGCGAGAGAAATTGC, CCACTTTCCGTTCAAGGTCAAG).

Human primer sequences:

CDH1 (TGCCCAGAAAATGAAAAAGG, GTGTATGTGGCAATGCGTTC),

VIM (GAGAACTTTGCCGTTGAAGC, GCTTCCTGTAGGTGGCAATC),

FN1 (CAGTGGGAGACCTCGAGAAG, TCCCTCGGAACATCAGAAAC).

Shared murine and human primer sequences:

GAPDH (GACCCCTTCATTGACCTCAAC, CTTCTCCATGGTGGTGAAGA).

shRNA sequences

pSP108 lentiviral target sequences:

shTwist1 #3, AAGCTGAGCAAGATTCAGACC.

shTwist1 #5, AGGTACATCGACTTCCTGTAC.

shControl (shGFP), GCAAGCTGACCCTGAAG.

pLKO.1 (Sigma-Aldrich) lentiviral target sequences:

shG3BP2 #2, AGTTAAATTGAGGTGGACATT.

shG3BP2 #5, TTCGAGGAGAAGTACGTTTAA.

shG3BP2 #6, CGGGAGTTTGTGAGGCAATAT.

shG3BP2 #8, CCACAAAGTATTATCTCTGAA.

Supplementary Material

Refer to Web version on PubMed Central for supplementary material.

Author Manuscript Author Manuscript Author Manuscript Author Manuscript

Acknowledgments

We thank members of the Yang lab, especially Mark Eckert, for helpful discussions. We thank the UCSD Shared Microscope Facility (P30NS047101), the UCSD Cancer Center Support Grant P30CA23100, and the NCI Cancer Diagnosis Program (CDP) for providing breast tumour tissue microarrays. The shRFP control pLKO.1 plasmid was a kind gift from S. Stewart. This work was supported by grants from NIH (DP2OD002420-01, 1RO1CA168689), DOD Breast Cancer Program W81XWH-13-1-0132, and ACS (RSG-09-282-01-CSM) to J.Y., from DOD W81XWH-13-1-0133 to A.J.E, from NIH (DK54441) and HHMI to S.S.T, and from NIH (P01AG007996) to R.L.S. S.C.W. was supported by a NIH Cancer Cell Biology Training grant (2T32CA067754), NIH Molecular Pathology of Cancer Training grant (5T32CA077109), and was an ARCS Foundation Scholar. L.F. was supported by a postdoctoral fellowship from Fondation pour la Recherche Médicale (SPE20130326547).

References

1. Paszek MJ, et al. Tensional homeostasis and the malignant phenotype. Cancer Cell. 2005; 8:241–254. [PubMed: 16169468]
2. Levental KR, et al. Matrix crosslinking forces tumor progression by enhancing integrin signaling. Cell. 2009; 139:891–906. [PubMed: 19931152]
3. Jaalouk DE, Lammerding J. Mechanotransduction gone awry. Nat Rev Mol Cell Biol. 2009; 10:63–73. [PubMed: 19197333]
4. Calvo F, et al. Mechanotransduction and YAP-dependent matrix remodelling is required for the generation and maintenance of cancer-associated fibroblasts. Nat Cell Biol. 2013; 15:637–646. [PubMed: 23708000]
5. Butcher DT, Alliston T, Weaver VM. A tense situation: forcing tumour progression. Nat Rev Cancer. 2009; 9:108–122. [PubMed: 19165226]
6. Colpaert C, Vermeulen P, Van Marck E, Dirix L. The presence of a fibrotic focus is an independent predictor of early metastasis in lymph node-negative breast cancer patients. Am J Surg Pathol. 2001; 25:1557–1558. [PubMed: 11717549]
7. Hasebe T, et al. Prognostic significance of fibrotic focus in invasive ductal carcinoma of the breast: a prospective observational study. Modern Pathology. 2002; 15:502–516. [PubMed: 12011255]
8. Conklin MW, et al. Aligned collagen is a prognostic signature for survival in human breast carcinoma. Am J Pathol. 2011; 178:1221–1232. [PubMed: 21356373]
9. Engler AJ, Humbert PO, Wehrle-Haller B, Weaver VM. Multiscale modeling of form and function. Science. 2009; 324:208–212. [PubMed: 19359578]
10. DuFort CC, Paszek MJ, Weaver VM. Balancing forces: architectural control of mechanotransduction. Nat Rev Mol Cell Biol. 2011; 12:308–319. [PubMed: 21508987]
11. Hoffman BD, Grashoff C, Schwartz MA. Dynamic molecular processes mediate cellular mechanotransduction. Nature. 2011; 475:316–323. [PubMed: 21776077]
12. Engler AJ, Sen S, Sweeney HL, Discher DE. Matrix elasticity directs stem cell lineage specification. Cell. 2006; 126:677–689. [PubMed: 16923388]
13. Dupont S, et al. Role of YAP/TAZ in mechanotransduction. Nature. 2011; 474:179–183. [PubMed: 21654799]
14. Yang J, Weinberg RA. Epithelial-mesenchymal transition: at the crossroads of development and tumor metastasis. Dev Cell. 2008; 14:818–829. [PubMed: 18539112]
15. Thiery JP, Acloque H, Huang RY, Nieto MA. Epithelial-mesenchymal transitions in development and disease. Cell. 2009; 139:871–890. [PubMed: 19945376]
16. Yang J, et al. Twist, a master regulator of morphogenesis, plays an essential role in tumor metastasis. Cell. 2004; 117:927–939. [PubMed: 15210113]
17. Fang X, et al. Twist2 contributes to breast cancer progression by promoting an epithelial-mesenchymal transition and cancer stem-like cell self-renewal. Oncogene. 2011; 30:4707–4720. [PubMed: 21602879]
18. Batlle E, et al. The transcription factor snail is a repressor of E-cadherin gene expression in epithelial tumour cells. Nat Cell Biol. 2000; 2:84–89. [PubMed: 10655587]
19. Cano A, et al. The transcription factor snail controls epithelial-mesenchymal transitions by repressing E-cadherin expression. Nat Cell Biol. 2000; 2:76–83. [PubMed: 10655586]

Author Manuscript Author Manuscript Author Manuscript Author Manuscript

20. Hajra KM, Chen DY, Fearon ER. The SLUG zinc-finger protein represses E-cadherin in breast cancer. Cancer Res. 2002; 62:1613–1618. [PubMed: 11912130]
21. Comijn J, et al. The two-handed E box binding zinc finger protein SIP1 downregulates E-cadherin and induces invasion. Mol Cell. 2001; 7:1267–1278. [PubMed: 11430829]
22. Eger A, et al. DeltaEF1 is a transcriptional repressor of E-cadherin and regulates epithelial plasticity in breast cancer cells. Oncogene. 2005; 24:2375–2385. [PubMed: 15674322]
23. Yang J, et al. Twist, a master regulator of morphogenesis, plays an essential role in tumor metastasis. Cell. 2004; 117:927–939. [PubMed: 15210113]
24. Eckert MA, et al. Twist1-induced invadopodia formation promotes tumor metastasis. Cancer Cell. 2011; 19:372–386. [PubMed: 21397860]
25. Desprat N, Supatto W, Pouille PA, Beaurepaire E, Farge E. Tissue deformation modulates twist expression to determine anterior midgut differentiation in Drosophila embryos. Dev Cell. 2008; 15:470–477. [PubMed: 18804441]
26. Johnson KR, Leight JL, Weaver VM. Demystifying the effects of a three-dimensional microenvironment in tissue morphogenesis. Methods Cell Biol. 2007; 83:547–583. [PubMed: 17613324]
27. Bissell MJ, Radisky DC, Rizki A, Weaver VM, Petersen OW. The organizing principle: microenvironmental influences in the normal and malignant breast. Differentiation. 2002; 70:537–546. [PubMed: 12492495]
28. Lee GY, Kenny PA, Lee EH, Bissell MJ. Three-dimensional culture models of normal and malignant breast epithelial cells. Nat Methods. 2007; 4:359–365. [PubMed: 17396127]
29. Debnath J, Muthuswamy SK, Brugge JS. Morphogenesis and oncogenesis of MCF-10A mammary epithelial acini grown in three-dimensional basement membrane cultures. Methods. 2003; 30:256–268. [PubMed: 12798140]
30. Xu Y, et al. Inducible knockout of Twist1 in young and adult mice prolongs hair growth cycle and has mild effects on general health, supporting Twist1 as a preferential cancer target. Am J Pathol. 2013; 183:1281–1292. [PubMed: 23906809]
31. Blick T, et al. Epithelial mesenchymal transition traits in human breast cancer cell lines. Clin Exp Metastasis. 2008; 25:629–642. [PubMed: 18461285]
32. Tran DD, Corsa CA, Biswas H, Aft RL, Longmore GD. Temporal and spatial cooperation of Snail1 and Twist1 during epithelial-mesenchymal transition predicts for human breast cancer recurrence. Mol Cancer Res. 2011; 9:1644–1657. [PubMed: 22006115]
33. Provenzano PP, et al. Collagen reorganization at the tumor-stromal interface facilitates local invasion. BMC Med. 2006; 4:38. [PubMed: 17190588]
34. Xu J, Lamouille S, Derynck R. TGF-beta-induced epithelial to mesenchymal transition. Cell Res. 2009; 19:156–172. [PubMed: 19153598]
35. Leight JL, Wozniak MA, Chen S, Lynch ML, Chen CS. Matrix rigidity regulates a switch between TGF-beta1-induced apoptosis and epithelial-mesenchymal transition. Mol Biol Cell. 2012; 23:781–791. [PubMed: 22238361]
36. Friedland JC, Lee MH, Boettiger D. Mechanically activated integrin switch controls alpha5beta1 function. Science. 2009; 323:642–644. [PubMed: 19179533]
37. Zhao B, et al. Inactivation of YAP oncoprotein by the Hippo pathway is involved in cell contact inhibition and tissue growth control. Genes Dev. 2007; 21:2747–2761. [PubMed: 17974916]
38. Kudo N, et al. Leptomycin B inactivates CRM1/exportin 1 by covalent modification at a cysteine residue in the central conserved region. Proc Natl Acad Sci U S A. 1999; 96:9112–9117. [PubMed: 10430904]
39. Singh S, Gramolini AO. Characterization of sequences in human TWIST required for nuclear localization. BMC Cell Biol. 2009; 10:47. [PubMed: 19534813]
40. Kim MM, Wiederschain D, Kennedy D, Hansen E, Yuan ZM. Modulation of p53 and MDM2 activity by novel interaction with Ras-GAP binding proteins (G3BP). Oncogene. 2007; 26:4209–4215. [PubMed: 17297477]
41. Prigent M, Barlat I, Langen H, Dargemont C. IkappaBalpha and IkappaBalpha /NF-kappa B complexes are retained in the cytoplasm through interaction with a novel partner, RasGAP SH3-binding protein 2. J Biol Chem. 2000; 275:36441–36449. [PubMed: 10969074]

Author Manuscript Author Manuscript Author Manuscript Author Manuscript

42. Wu HY, et al. Combining alkaline phosphatase treatment and hybrid linear ion trap/Orbitrap high mass accuracy liquid chromatography-mass spectrometry data for the efficient and confident identification of protein phosphorylation. Anal Chem. 2009; 81:7778–7787. [PubMed: 19702290]
43. Casas E, et al. Snail2 is an essential mediator of Twist1-induced epithelial mesenchymal transition and metastasis. Cancer Res. 2011; 71:245–254. [PubMed: 21199805]
44. Miller FR, Santner SJ, Tait L, Dawson PJ. MCF10DCIS. com xenograft model of human comedo ductal carcinoma in situ J Natl Cancer Inst. 2000; 92:1185–1186.
45. Kakkad SM, et al. Collagen I fiber density increases in lymph node positive breast cancers: pilot study. J Biomed Opt. 2012; 17:116017. [PubMed: 23117811]
46. Provenzano PP, et al. Collagen density promotes mammary tumor initiation and progression. BMC Med. 2008; 6:11. [PubMed: 18442412]
47. DuFort CC, Paszek MJ, Weaver VM. Balancing forces: architectural control of mechanotransduction. Nat Rev Mol Cell Biol. 2011; 12:308–319. [PubMed: 21508987]
48. Alexander NR, et al. N-cadherin gene expression in prostate carcinoma is modulated by integrin-dependent nuclear translocation of Twist1. Cancer Res. 2006; 66:3365–3369. [PubMed: 16585154]
49. Chaudhuri T, Rehfeldt F, Sweeney HL, Discher DE. Preparation of collagen-coated gels that maximize in vitro myogenesis of stem cells by matching the lateral elasticity of in vivo muscle. Methods Mol Biol. 2010; 621:185–202. [PubMed: 20405368]
50. Klenova E, Chernukhin I, Inoue T, Shamsuddin S, Norton J. Immunoprecipitation techniques for the analysis of transcription factor complexes. Methods. 2002; 26:254–259. [PubMed: 12054881]
51. Guo Y, Ma SF, Grigoryev D, Van Eyk J, Garcia JG. 1-DE MS and 2-D LC-MS analysis of the mouse bronchoalveolar lavage proteome. Proteomics. 2005; 5:4608–4624. [PubMed: 16240291]
52. Artimo P, et al. ExPASy: SIB bioinformatics resource portal. Nucleic Acids Res. 2012; 40:W597–603. [PubMed: 22661580]

Author Manuscript

Author Manuscript

Author Manuscript

Author Manuscript

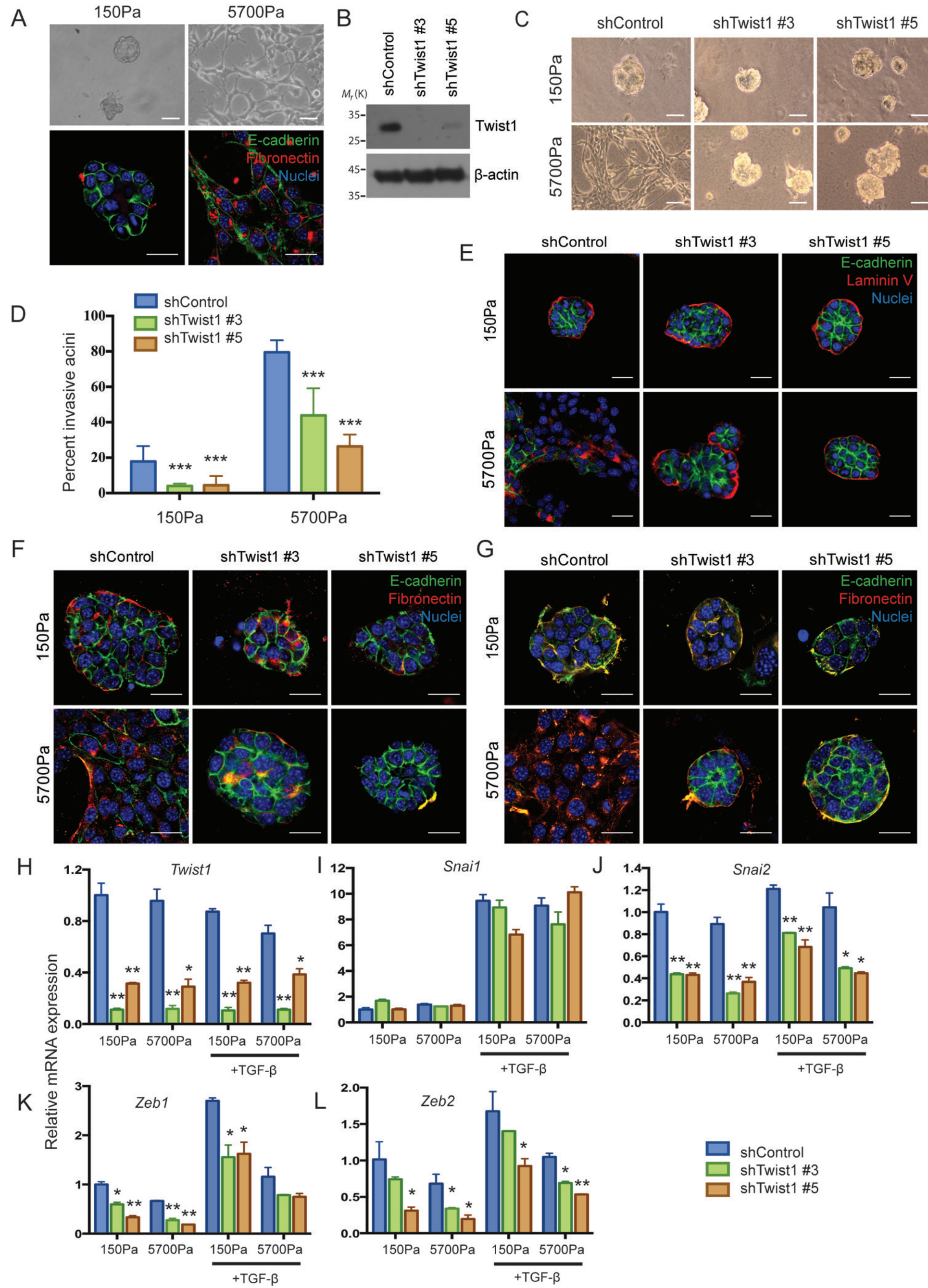

Figure 1. TWIST1 is essential for matrix-stiffness-induced EMT and invasion

(a) Eph4Ras cells after 5 days of growth in 3D culture on polyacrylamide hydrogels with the indicated rigidities imaged by bright-field (top) or stained (bottom) for E-cadherin (green), fibronectin (red) and nuclei (blue; scale bars, 25μm). **(b)** Cell lysates from Eph4Ras cells expressing control and *Twist1* shRNAs were analysed by SDS–PAGE and probed for *Twist1* and β-actin. Unprocessed original scans of the blots are shown in Supplementary Fig. 7. **(c)** Bright-field images of Eph4Ras cells expressing control or *Twist1* knockdown shRNAs after 5 days growth in 3D culture on polyacrylamide hydrogels with the indicated rigidities (scale

Author Manuscript
Author Manuscript
Author Manuscript
Author Manuscript

bars, 50 μm). **(d)** Quantification of invasive acini in 3D culture described in c from 3 independent experiments (***, P < 0.001, unpaired two-tailed t -test with Welch's correction, n = 50 acini per experiment, 3 independent experiments, error bars represent s.d.). **(e)** Eph4Ras cells expressing control or *Twist1* knockdown shRNAs after 5 days growth in 3D culture on polyacrylamide hydrogels with the indicated rigidities stained for laminin V (red), E-cadherin (green) and nuclei (blue; scale bars, 25 μm). **(f,g)** Eph4Ras cells expressing control or *Twist1* shRNAs were cultured in 3D culture with the indicated rigidities in the absence **(f)** or presence of 5ngml−1 TGF-β **(g)** for 8 days and stained for E-cadherin (green), fibronectin (red) and nuclei (blue; scale bars, 25μm). **(h–l)** qPCR analysis of *Twist1* (**h**), *Snai1* (**i**), *Snai2* (**j**), *Zeb1* (**k**) and *Zeb2* (**l**) mRNA expression in Eph4Ras cells expressing control or *Twist1* shRNAs cultured under the indicated matrix rigidities in the absence or presence of 5 ng ml−1 TGF-β (*, P < 0.05; **, P < 0.01; unpaired two-tailed t -test with Welch's correction, n = 3 independent experiments, statistics source data can be found in Supplementary Table 1; error bars represent s.d.).

Author Manuscript Author Manuscript Author Manuscript Author Manuscript

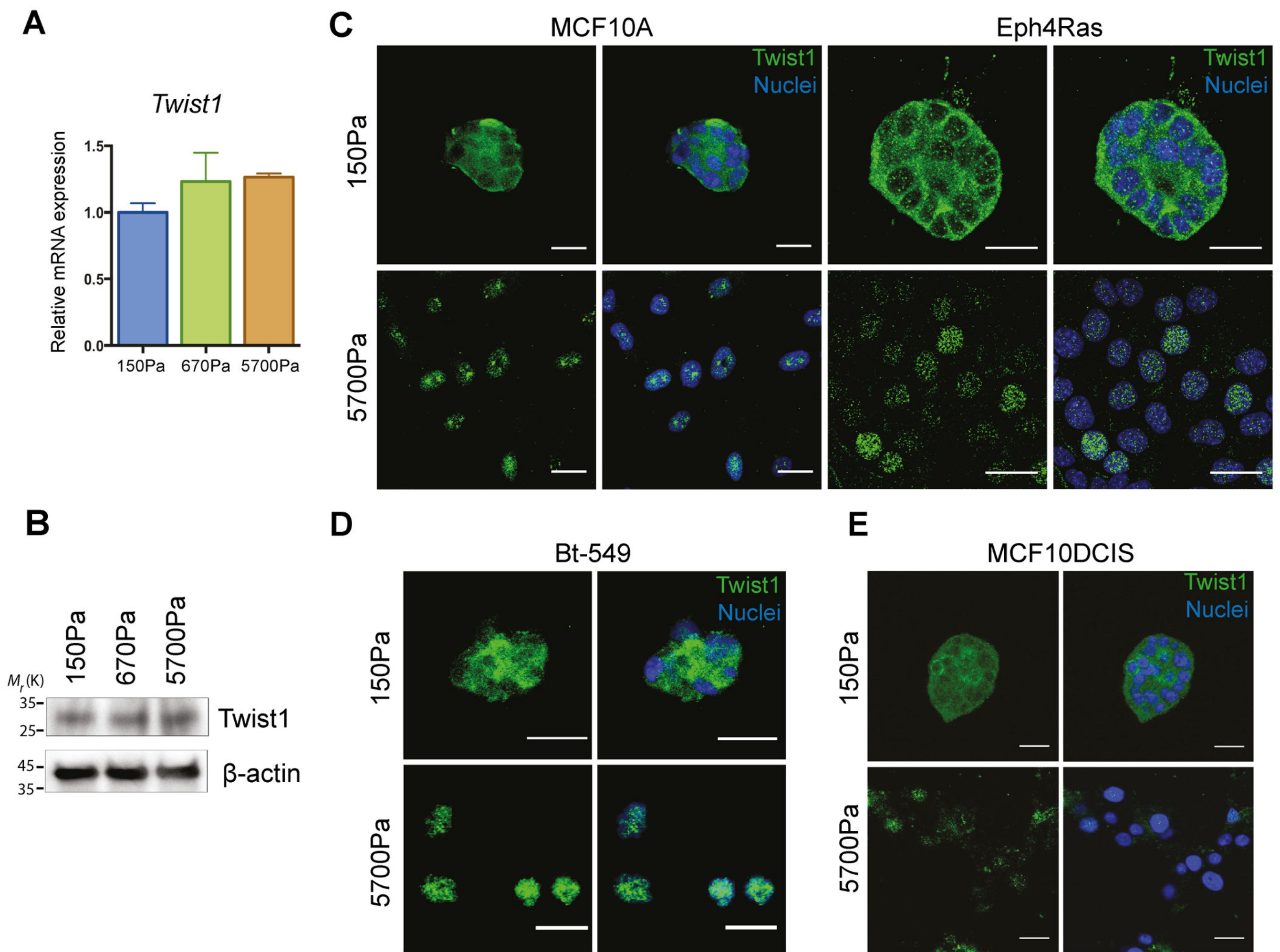

Figure 2. Matrix stiffness regulates TWIST1 nuclear localization

(a) qPCR analysis of MCF10A cells grown in 3D culture on polyacrylamide hydrogels with the indicated rigidities (not significant, unpaired two-tailed t-test with Welch's correction, n = 3 independent experiments, statistics source data can be found in Supplementary Table 1; error bars represent s.d.). **(b)** Cell lysates from MCF10A cells grown in 3D culture on polyacrylamide hydrogels with the indicated rigidities were analysed by SDS–PAGE and probed for TWIST1 and β-actin. Unprocessed original scans of the blots are shown in Supplementary Fig. 7. **(c–e)** Eph4Ras, MCF10A **(c)**, Bt-549 **(d)** and MCF10DCIS **(e)** cells were cultured in 3D culture with the indicated rigidities for 5 days and stained for TWIST1 (green) and nuclei (blue; scale bars, 25 μm)

Author Manuscript Author Manuscript Author Manuscript Author Manuscript

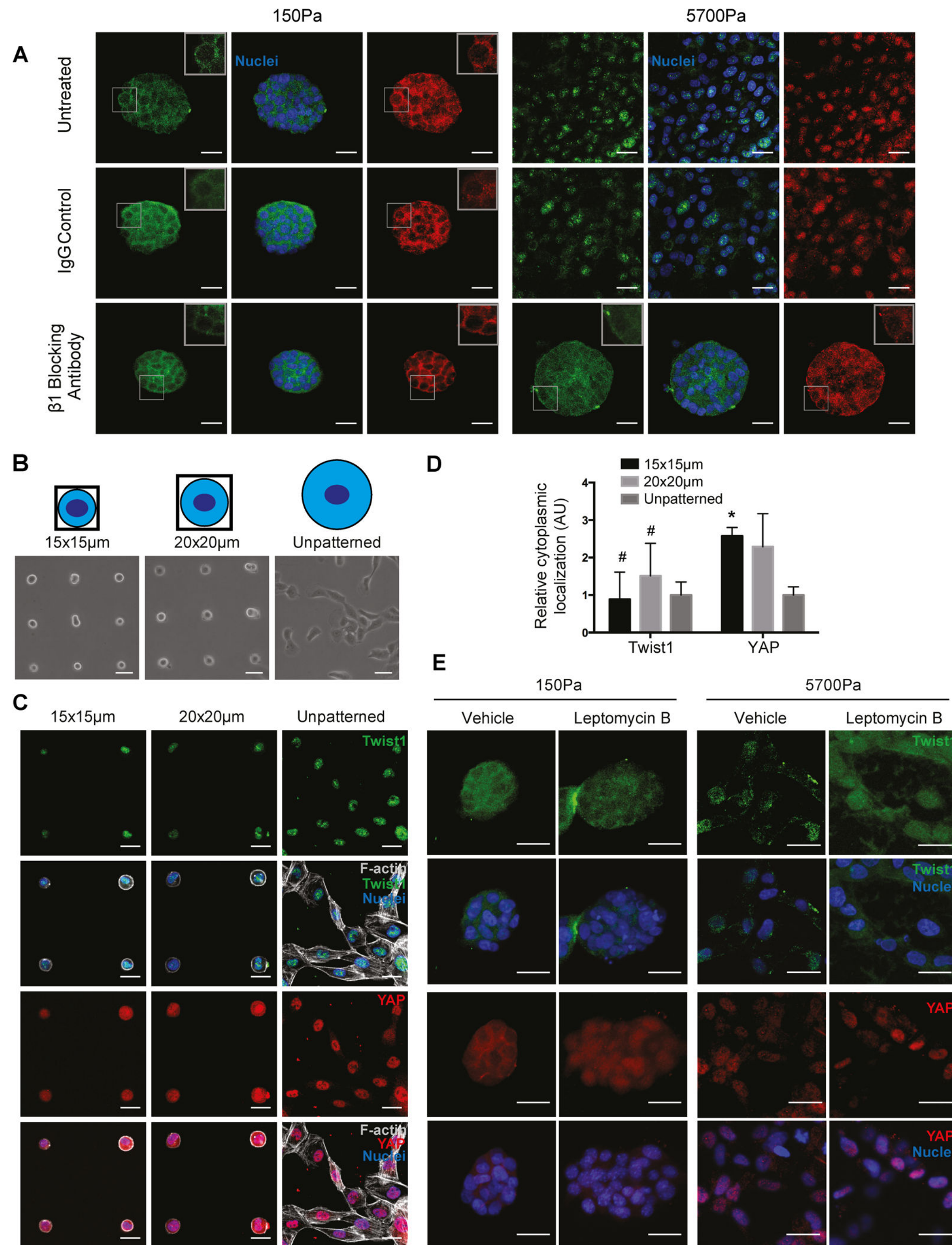

Figure 3. TWIST1 and YAP nuclear localization are regulated by distinct mechanotransduction pathways

(a) MCF10A cells were cultured in 3D culture on polyacrylamide hydrogels with the indicated rigidities in the presence of a control IgG or a β1-integrin-blocking antibody (AIIB2) for 5 days and stained for TWIST1 (green), YAP (red) and nuclei (blue; scale bars, 25 μm). **(b,c)** Bright-field images (scale bars, 50 μm; b) and confocal images of MCF10A cells cultured on micropatterned glass coverslips for 6h stained for TWIST1 (green), YAP (red), F-actin (greyscale) and nuclei (blue; scale bars, 25μm; c). **(d)** Quantification of

Author Manuscript

Author Manuscript

Author Manuscript

Author Manuscript

relative cytoplasmic localized TWIST1 and YAP. (#, not significant; *, $P < 0.01$, unpaired two-tailed t -test with Welch's correction, $n = 25$ cells per experiment, 3 independent experiments, error bars represent s.d.). **(e)** MCF10A cells were cultured in 3D culture on polyacrylamide hydrogels with the indicated rigidities in the absence or presence of leptomycin B and stained for TWIST1 (green), YAP (red) and nuclei (blue; scale bars, 25 μm).

Author Manuscript Author Manuscript Author Manuscript Author Manuscript

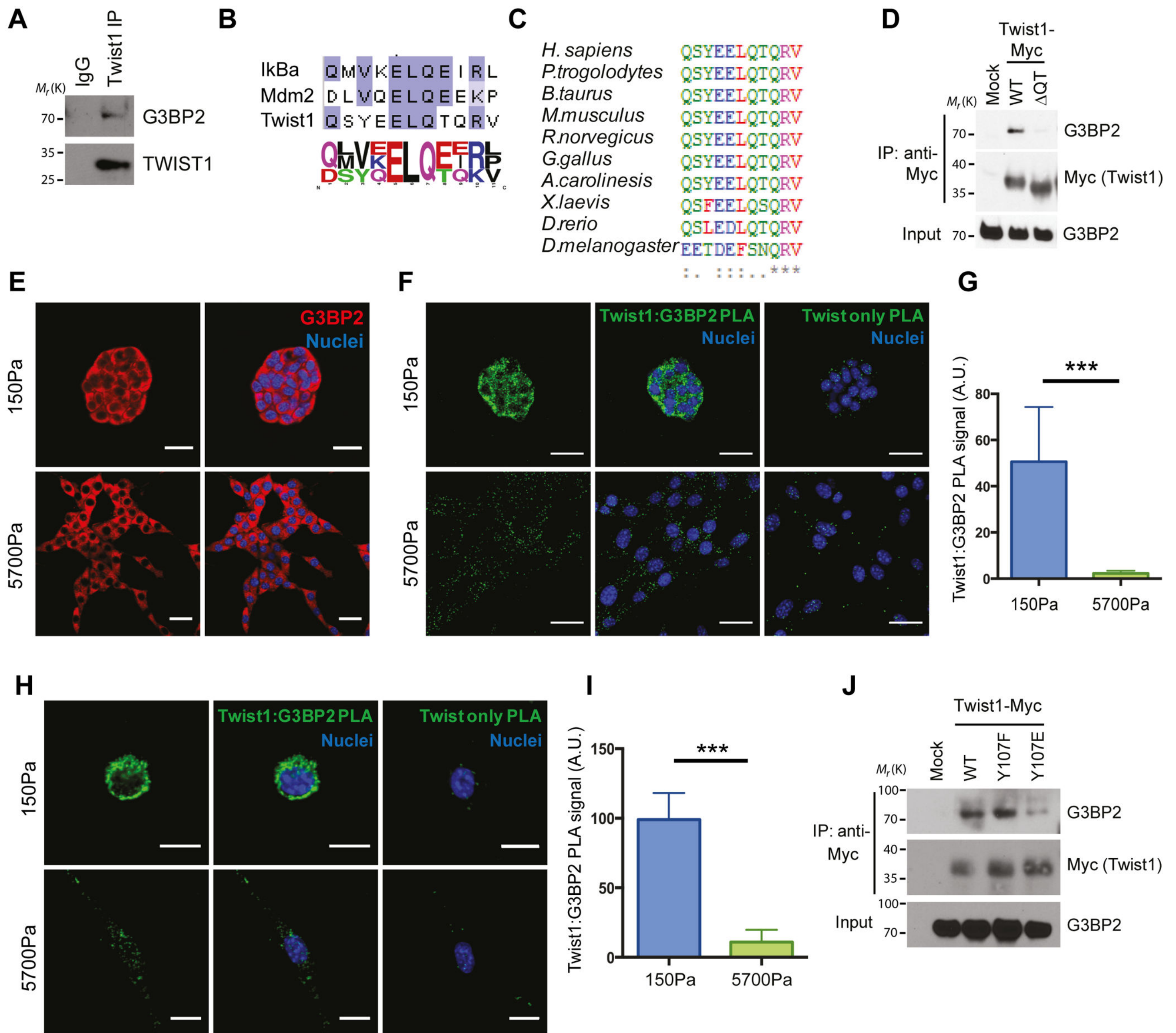

Figure 4. Matrix stiffness regulates the interaction between TWIST1 and G3BP2 to control TWIST1 subcellular localization

(a) Endogenous TWIST1 from MCF10A cell lysates was immunoprecipitated, analysed by SDS–PAGE and probed for G3BP2 and TWIST1. **(b)** Population plot of the putative G3BP2-binding domain motif. **(c)** Alignment of the putative G3BP2-binding domain in TWIST1 homologues. **(d)** Exogenously expressed wild-type (WT) and Gln105-Thr112 deletion (QT) Myc-tagged Twist1 from 293T cell lysates were immunoprecipitated, analysed by SDS–PAGE and probed for G3BP2 and Myc. **(e)** Eph4Ras cells in 3D culture at the indicated rigidities were stained for G3BP2 (red) and nuclei (blue; scale bars, 50 μm). **(f)** Eph4Ras cells in 3D culture for 6 days at the indicated rigidities were analysed for Twist1 and G3bp2 interaction by in situ PLA assay, PLA signal (green) and DAPI (blue; scale bars, 25 μm. **(g)** Quantification of PLA signal normalized to cell number in 3D cultures described

in f (***, P < 0.001, unpaired two-tailed t -test with Welch's correction, n = 50 acini, 3 independent experiments, error bars represent s.d.). **(h)** Eph4Ras cells in 3D culture for 20h at the indicated rigidities were analysed for Twist1 and G3bp2 interaction by in situ PLA assay, PLA signal (green) and DAPI(blue; scale bars, 15μm). **(i)** Quantification of PLA signal normalized to cell number in 3D cultures described in h (***, P < 0.001, unpaired two-tailed t -test with Welch's correction, n = 25 acini, 3 independent experiments, error bars represent s.d.). **(j)** Exogenously expressed wild- type (WT), Y107F and Y107E Myc-tagged Twist1 from 293T cell lysates were immunoprecipitated and analysed by SDS–PAGE, and probed for G3BP2 and Myc. Unprocessed original scans of the blots are shown in Supplementary Fig. 7.

Author Manuscript
Author Manuscript
Author Manuscript
Author Manuscript

Author Manuscript
Author Manuscript
Author Manuscript
Author Manuscript

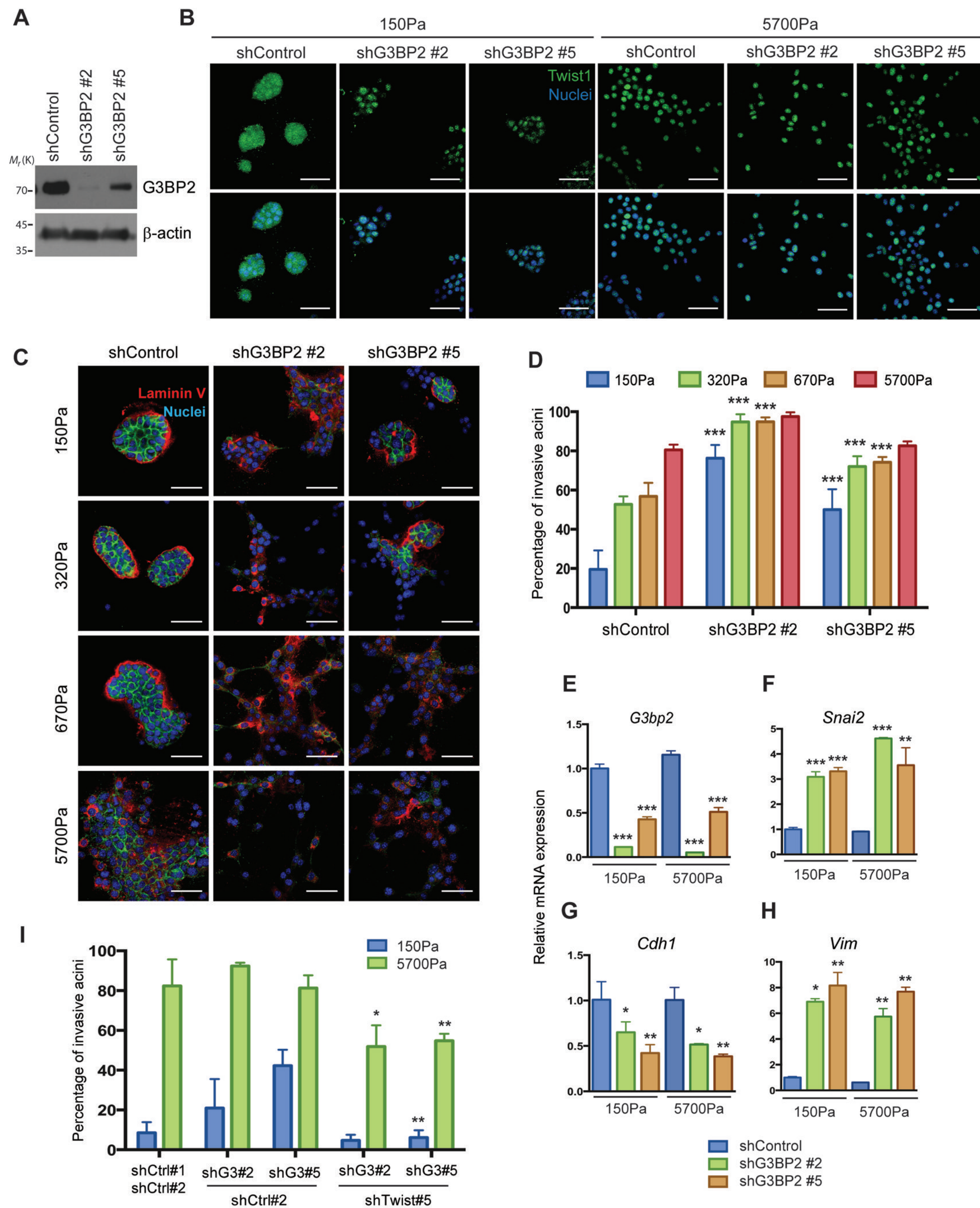

Figure 5. Loss of G3BP2 cooperates with increasing matrix stiffness to promote TWIST1 nuclear localization and EMT

(a) Cell lysates from Eph4Ras cells expressing control or *G3bp2* shRNAs were analysed by SDS–PAGE and probed for G3BP2 and β-actin. Unprocessed original scans of the blots are shown in Supplementary Fig. 7. **(b)** Eph4Ras cells expressing control or *G3bp2* shRNAs were cultured in 3D culture with the indicated rigidities for 5 days and stained for Twist1 (green) and nuclei (blue; scale bars, 50 μm). **(c)** Eph4Ras cells expressing control or *G3bp2* shRNAs were cultured in 3D culture with varying rigidities for 5 days and stained for E-

Author Manuscript Author Manuscript Author Manuscript Author Manuscript

cadherin (green), laminin V (red) and nuclei (blue; scale bars, 50μm). **(d)** Quantification of invasive acini in 3D culture described in c from 3 independent experiments (***, P < 0.001, unpaired two-tailed t -test with Welch's correction, n = 50 acini per experiment, 3 independent experiments, error bars represent s.d.). **(e–h)** qPCR analysis of *G3bp2* **(e)**, *Snai2* **(f)**, *Cdh1* **(g)** and *Vim* **(h)** in Eph4Ras cells expressing control or *G3bp2* shRNAs 3D cultured under the indicated matrix rigidities for 5 days (*, P < 0.05; **, P < 0.01; ***, P < 0.001, unpaired two-tailed t -test with Welch's correction, n = 4 independent experiments, Supplementary Table 1, error bars represent s.d.). **(i)** Quantification of invasive acini of Eph4Ras cells expressing control (Ctrl shRNA1) or *G3bp2* shRNAs, together with control (Ctrl shRNA2) or *Twist1* shRNA (*Twist1* shRNA5), 3D cultured under the indicated matrix rigidities for 5 days, from 3 independent experiments (*, P < 0.05; **, P < 0.01, unpaired two-tailed t -test with Welch's correction, n = 50 acini per experiment, 3 independent experiments; double knockdown compared with the respective single knockdown, error bars represent s.d.).

Author Manuscript Author Manuscript Author Manuscript Author Manuscript

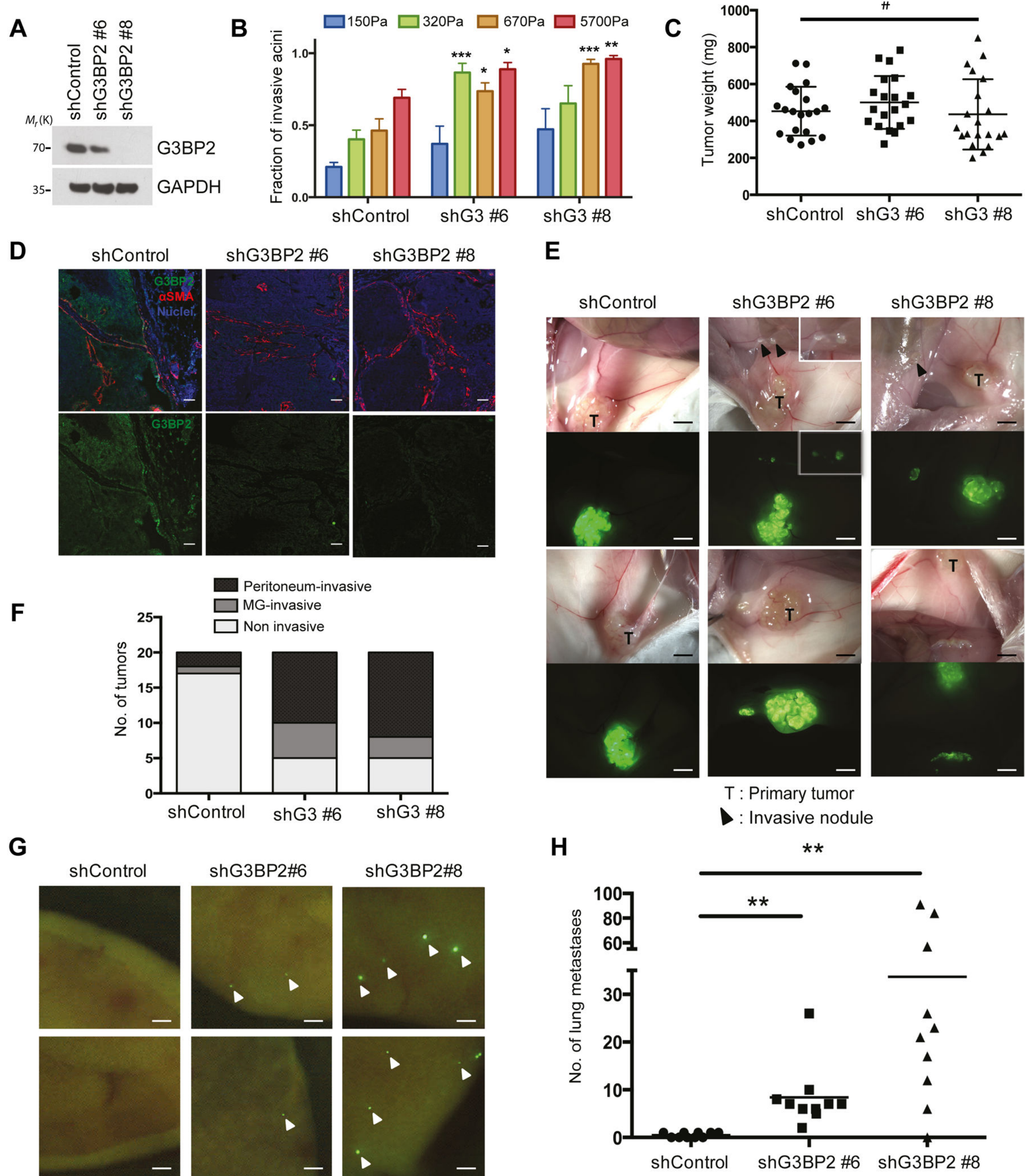

Figure 6. Loss of G3BP2 induces tumour invasion *in vivo*

(a) Cell lysates from MCF10DCIS cells expressing control or *G3BP2* shRNAs were analysed by SDS–PAGE and probed for G3BP2 and GAPDH. Unprocessed original scans of the blots are shown in Supplementary Fig. 7. **(b)** Quantification of invasive acini formed by MCF10DCIS cells expressing control or *G3BP2* shRNAs cultured in 3D culture with varying rigidities for 5 days (*, $P < 0.05$; **, $P < 0.01$; ***, $P < 0.001$, unpaired two-tailed t -test with Welch's correction, n = 50 acini per experiment, 3 independent experiments; error bars denote s.e.m.). **(c)** Tumour weight of MCF10DCIS xenograft tumours expressing

Author Manuscript Author Manuscript Author Manuscript Author Manuscript

control or *G3BP2* shRNAs (#, not statistically significant, unpaired two-tailed t -test with Welch's correction, n = 20 tumours from 10 mice per group, 3 independent experiments, error bars represent s.d.). **(d)** Tissue sections of control and *G3BP2* shRNA MCF10DCIS xenografts stained for G3BP2 (green), αSMA (red) and nuclei (blue) and imaged by confocal microscopy (scale bars, 50μm). **(e)** Fluorescent and bright-field images of GFP (green)-labelled MCF10DCIS xenograft tumours *in situ* (scale bars, 5 mm). **(f)** Quantification of local (MG-invasive) and regional (Peritoneum-invasive) invasion of MCF10DCIS xenograft tumours. **(g,h)** Fluorescent images (scale bars, 100 μm; g) and quantification **(h)** of lung metastases (green, indicated by arrows) from MCF10DCIS xenograft tumours (**, $P < 0.01$, unpaired correction, n = 10 mice per experiment, two-tailed t -test with Welch's 3 independent experiments).

Author Manuscript
Author Manuscript
Author Manuscript
Author Manuscript

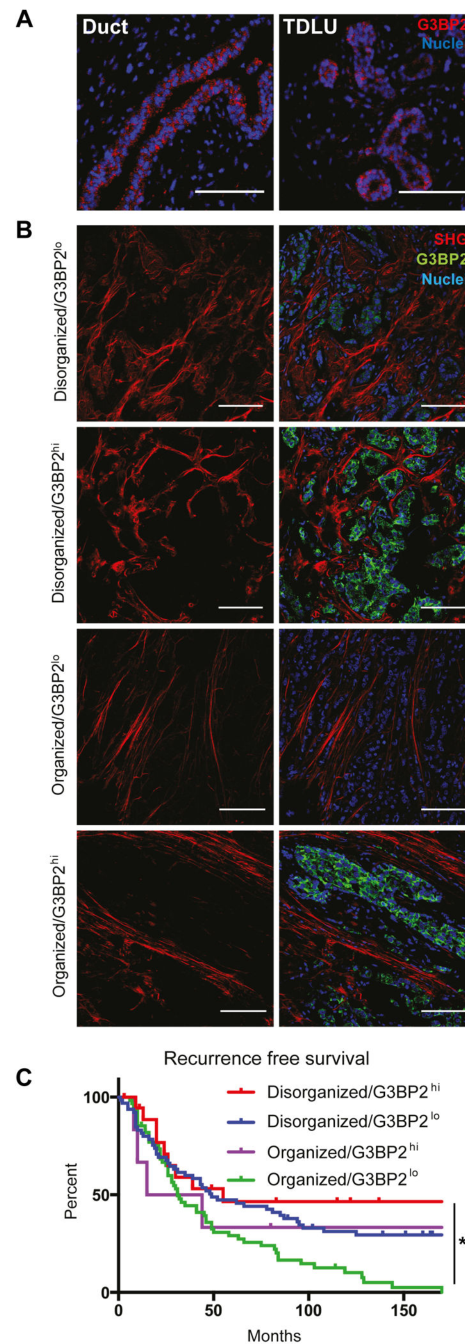

Figure 7. Downregulation of G3BP2 and increasing collagen organization synergistically predict poor outcome in breast cancer patients

(a) Confocal microscopy of normal human breast terminal ductal lobular units (TDLU) and ducts stained for G3BP2 (red) and nuclei (blue; scale bars, 100 μm). **(b)** Rep- resentative images of stage-3 human breast tumours analysed for collagen organization by SHG (red), and stained for G3BP2 (green) and TO-PRO-3 for nuclei (blue) respectively (scale bars, 100μm). **(c)** Kaplan–Meier curve of recurrence-free survival for stage-3 breast cancer patients, stratified by collagen organization (SHG) and G3BP2 expression (*, Disorganized

collagen/G3BP2^{high} tumours versus Organized collagen/G3BP2^{low}, log-rank P value = 0.0135, n = 152 breast tumours; Disorganized collagen/G3BP2^{high} n = 19 breast tumours; Disorganized collagen/G3BP2^{low} n = 65 breast tumours; Organized collagen/G3BP2^{high} n = 6 breast tumours; Disorganized collagen/G3BP2^{low} n = 62 breast tumours).

Author Manuscript Author Manuscript Author Manuscript Author Manuscript